Combustion and Flame 229 (2021) 111366

Contents lists available at ScienceDirect

Combustion and Flame

journal homepage: www.elsevier.com/locate/combustflame

An evolutionary, data-driven approach for mechanism optimization: theory and application to ammonia combustion

A. Bertolino[a,b,c], M. Fürst[a,b,c], A. Stagni[c], A. Frassoldati[c], M. Pelucchi[c], C. Cavallotti[c], T. Faravelli[c], A. Parente[a,b,*]

[a] Université Libre de Bruxelles, Ecole polytechnique de Bruxelles, Aero-Thermo-Mechanics Laboratory, Bruxelles, Belgium
[b] Université Libre de Bruxelles and Vrije Universiteit Brussel, Combustion and Robust Optimization Group (BURN), Bruxelles, Belgium
[c] Department of Chemistry, Materials, and Chemical Engineering "G. Natta", Politecnico di Milano, Milano 20133, Italy

ARTICLE INFO

Article history:
Received 18 October 2020
Revised 8 February 2021
Accepted 9 February 2021
Available online 9 March 2021

Keywords:
Optimization
Detailed kinetics
Ammonia
Uncertainty quantification

ABSTRACT

In this work, we propose a novel data-driven approach for detailed kinetic mechanisms optimization. The approach is founded on a curve matching-based objective function and includes a methodology for the optimisation of pressure-dependent reactions via logarithmic interpolation (PLOG format). In order to highlight the advantages of the new formulation of the objective function, a comparison with L_1 and L_2 norm is performed. The selection of impactful reactions is carried out by introducing a Cumulative Impact Function (CIF), while an Evolutionary Algorithm (EA) is adopted for the optimization. The capabilities of the proposed methodology were demonstrated using a database of ~635 experimental datapoints on ammonia combustion, covering standard targets like ignition delay times, speciation and laminar flame speed. The optimization was carried out starting from a recently published mechanism, describing ammonia pyrolysis and oxidation, largely developed using first-principles calculation of rate constants. After the selection of the 24 most impactful reactions, the related 101 normalized Arrhenius parameters were simultaneously varied, within their uncertainty bounds. Their uncertainty bounds were taken from the literature, when available, or estimated according to the level of theory adopted for the determination of the rate constant. Hence, we also provide guidelines to estimate uncertainty for reaction rate constants derived from first principles calculations using well consolidated computational protocols as a reference. The optimized mechanism was found to improve the nominal one, showing a satisfactory agreement over the entire range of operating conditions. Moreover, the use of 'curve matching' indices was found to outperform the adoption of L_1 and L_2 norms. The comparison between the nominal mechanism and the one optimized via curve matching allowed a clear identification of different critical reaction pathways for different experimental targets. From this perspective, the methodology proposed herein can find further application as a useful design-of-experiments tool for an accurate evaluation of crucial kinetic constants, thus driving further mechanism improvement.

1. Introduction

The development of detailed kinetic mechanisms for fuels combustion supports and facilitates the implementation of cleaner fuels and more efficient combustion technologies, in the perspective of a reduced environmental impact, a differentiation of energy sources and their wiser utilization [1]. From a chemical kinetics perspective, a combustion process involves a considerable amount of species connected by a complex network of reactions. The increase in computing capabilities and in the accuracy and availability of experimental data [2],[3] pushes the development of kinetic models of increasing complexity in terms of number of species (~10^3) and reactions (~10^4) [1]. The rate constants of these reactions constitute the parameters of such models, together with thermodynamic and transport properties. These can be determined experimentally, theoretically or based on analogy with similar compounds for which kinetic subsets already exist [4]. The last decade was characterized by a more frequent adoption of theoretical methods (e.g. ab initio transition state theory-based master

* Corresponding author at: Université Libre de Bruxelles, Ecole polytechnique de Bruxelles, Aero-Thermo-Mechanics Laboratory, Bruxelles, Belgium.
E-mail address: alessandro.parente@ulb.be (A. Parente).

https://doi.org/10.1016/j.combustflame.2021.02.012

Nomenclature

Roman symbols

A	pre-exponential factor [s – cm^3 – mol]
E_a	activation energy [cal/mol]
f_r	uncertainty factor for reaction r
R	universal gas constant [cal/mol/K]
d_j^0	zero-order derivative dissimilarity index for the *j*th dataset
d_j^1	first-order derivative dissimilarity index for the *j*th dataset
g	experimental data spline
m	model evaluations spline
p_c	cross-over rate
p_m	mutation rate
X	uniformly distributed random variable
Y	optimisation target
$I_{r,s}$	impact coefficient of r^{th} reaction in s^{th} test case
$s_{r,s}$	sensitivity coefficient of r^{th} reaction in s^{th} test case

Greek symbols

κ	kinetic rate constant [s – cm^3 – mol]
α	ln(A) [-]
β	temperature exponent [-]
ε	activation temperature (E_a/R) [K]

Acronyms

GRI	Gas Research Institute
B2B-DC	Bound to (2) Bound Data Collaboration
EA	Evolutionary Algorithm
GA	Genetic Algorithm
MUM-PCE	Method of Uncertainty Minimization using Polynomial Chaos Expansion
PLOG	Pressure LOGarithmic interpolation
CM	Curve Matching
RCM	Rapid Compression Machine
PFR	Plug Flow Reactor
JSR	Jet Stirred Reactor
FPF	Freely Propagating Flames
TC	Test Case
CSF	Cumulative Sensitivity Function
CIF	Cumulative Impact Function
PES	Potential Energy Surface

Subscripts

0	nominal
r	r^{th} reaction
max	maximum value of the related variable
min	minimum value of the related variable
L_2	dissimilarity index based on L_2 norm evaluation of given polynomials
p	Pearson based dissimilarity measure of given polynomials
m	mutation
c	cross-over

equation, AI-TST-ME) [5],[6], for the determination of kinetic parameters and thermodynamic properties. Beyond the intrinsic advantages derived from the massive use of AI-TST-ME methods in terms of model predictive capabilities, the increasing popularity of such methods is justified by improved theoretical methods and algorithms currently available, and by the capability of measuring rate constants for elementary steps in a more accurate way, thus providing an immediate validation target for the theoretical results. In addition, automated computational protocols implementing the state-of-the-art AI-TST-ME methods [7–11] are reaching out to a much wider audience, thus paving the way to a more standardized approach to theoretical calculations within the combustion chemistry community. Nonetheless, adopting the best rate parameters does not necessarily lead to improved model performances when looking at a wide range of experimental targets [4],[12]. This is due to multiple reasons: i) reference kinetic mechanisms within the combustion science and engineering community have a long and consolidated history, or, in machine learning terms, are "well-trained" models, iteratively validated over a wide range of experimental targets over decades of research activities [12],[13]. ii) Models that have been historically developed largely relying on analogy rules and on semi-empirical, or at least less complex, thermochemical kinetics principles [14] are typically self-consistent, even in terms of the very likely possibility of hiding error compensation phenomena. iii) Every rate constant, including those from theoretical methods, is affected by an uncertainty [12],[15],[16].

The implementation of theory-based development strategies is an iterative process that shows its payback only in the mid-to-long-term perspective. In fact, due to the hierarchical nature of detailed mechanisms and their development [17], implementing one single accurate rate parameter, or new rate parameters for an entire reaction class, might strongly perturb the critical equilibrium between the different modules of a kinetic model. This is particularly important if, while gradually introducing new parameters from theoretical calculations, a well performing model is needed for applications of interest to the end-user.

Regarding theoretical determinations the uncertainty can be intuitively considered as decreasing with an increasing detail in the level of theory [18]. In the past, uncertainty propagation methods were used to quantify the level of uncertainty of phenomenological rate coefficients, in *n*-propyl radical oxidation, obtained from theory [19]. In recent times, quantum chemistry calculations are said to have reached a level of accuracy comparable to that of experimental measurements [5], promoting their applicability in combustion mechanism development [20]. A multi-scale modelling approach was proposed by Burke et al. [21],[22], who optimized a set of uncertain theoretical kinetics parameters directly relating their uncertainties to the combustion behaviour in terms of macroscopic targets (ignition delay time, laminar flame speed, etc.). Shannon et al. [23] proposed the use of experimental data and uncertainty quantification to constrain and optimize input parameters in the master equation using MESMER [24].

Essentially, each parameter of a kinetic model, expressed in any form, can be considered as a randomly distributed variable within its uncertainty range [16]. This feature can be exploited in mathematical optimization if the model is required to accurately perform on a small, as well as large, set of experimental targets.

Optimization is a powerful tool for data-driven mechanism development, which can be used in combination with the solution of the so called "inverse problem", consisting in obtaining a new set of constrained kinetic parameters, by minimizing or maximizing a chosen objective function using experimental data as targets.

In the context of chemical mechanisms, *Solution Mapping* [25] was the first method applied to a large, complex system. This method faces the multi-modality of the problem through polynomial response surfaces, and it was applied for the development of the GRI-MECH [26]. This mechanism was trained on 77 well-documented and heterogeneous experimental targets describing the combustion of natural gas. Frenklach et al. [27] introduced the concept of *collaboration of data*, and demonstrated that a joint analysis on the entire data sample can increase the amount of extracted information and improve the results. Feeley et al. [28] showed that the techniques of data collaboration can be used to rigorously assess the mutual consistency of experimental results and identify potential outliers, using a chemical kinetic

model. The methodology, called Bound-to-Bound Data Collaboration (B2B-DC) has been successfully applied and refined in several other works [29–34]. The applicability of Evolutionary/Genetic Algorithms (EA/GA) to optimization problems involving detailed kinetics was broadly investigated by Elliott et al. [35]. EA/GA were found particularly suitable for searching objective-function spaces characterized by high dimensionality. Turányi et al. [36] proposed a sum-of-squared-error-based methodology, accounting for both direct and indirect measurements, and successfully applied it to H_2/O_2 [37], $H_2/O_2/NO_x$ [38], H_2/CO mixtures [39], CH_2O and CH_3OH [40], and ethanol [41]. Najm et al. [42] applied forward Uncertainty Quantification (UQ) and Polynomial Chaos Expansion (PCE) to chemical kinetics. Sheen and Wang introduced the method of uncertainty minimization by polynomial chaos expansion (MUM-PCE) [43],[44]. Cai and Pitsch [45] minimized the uncertainty in a *n*-pentane combustion mechanism by applying the MUM-PCE method to the optimization of rate rules. They also proposed a strategy to optimize pressure-dependent reactions, formulated via logarithmic interpolation, i.e. PLOG standard [46]. PLOG expressions are indeed gradually substituting the previous formulation of pressure-dependent rate constants, as they yield a better fitting to experiments or calculations [5]. As this formalism uses accurate rates for discrete pressures, the parameters of each pressure value were considered independent from each other in [45].

The optimization of relatively compact kinetic mechanisms, such as methane, hydrogen, and ammonia is particularly attractive, because of i) the large availability of high-fidelity data [4], ii) the current interest in e-fuels produced from renewable energy [47], and iii) their compact size allowing to benchmark the suitability of different optimization algorithms before their application to more complex networks. Among them, the combustion kinetics of ammonia (NH_3) is one of the most active research fields, due to the high potential of ammonia as a fuel, from both an economic and a technical perspective [48]. Indeed, ammonia is a carbon-free energy vector with high hydrogen content, which can be liquefied at pressures higher than 9.9 bar at ambient temperature. Historically ammonia has been used as NO reducing agent in both selective and non-selective catalytic reduction. The importance of ammonia is also related to other renewable energy sources: for example, it is a by-product of anaerobic digestion of municipal wastewater sludges [49], and it is found in trace amounts in biogas [50]. The combined use of NH_3 with conventional fuels like H_2 or CH_4 has also been studied in order to improve shortcomings related to its low reactivity [51],[52]. Also, optimal operating conditions were found to minimize NO_x emissions [53]. Therefore, several mechanisms describing the oxidation of NH_3 and NH_3/H_2 fuel blends were developed [54–56]. Glarborg et al. [57] recently proposed a comprehensive nitrogen chemistry model, including ammonia itself. Anyway, uncertainties still persist in the characterization of ammonia chemistry for an accurate prediction of ignition, speciation, and laminar flame speed [57]. So far, optimization studies in chemical kinetics have been relying on objective functions based on the L1 and L2 norms of the difference between models predictions and corresponding experimental targets [35],[58],[59]. Recently, You et al. [31] minimized the L_1-norm of the difference between the active variables values and the nominal ones, constrained on the feasible set of combinations identified with B2B-DC [27]. The formulations in [31] not only improve the model performance, but also minimize the deviation of parameters values from the literature recommendations. Recently, Bernardi et al. [60] presented an innovative framework based on Curve Matching (CM), consisting in a multi-faceted functional analysis of the profiles obtained from both models and experiments. In this approach, they introduced a proper metric to quantify the similarity between the curves representing experiments and simulations, rather than a point-wise measure of the distance between them. Pelucchi et al. [61] revised and proposed such framework as a further step towards an automatic model validation protocol.

In this work, a novel methodology for the optimization of kinetic mechanisms is proposed, which includes, for the first time, the possibility to optimize PLOG reactions by accounting for interdependencies between rates at different pressures and the use of the CM index [61] as the objective function. The effectiveness of such approach was verified by adopting a kinetic mechanism for ammonia combustion as a case study [20]. This model was recently proposed and largely relies on theoretical calculations of key reaction rate constants. As an added value, this work also presents guidelines for attributing reasonable uncertainty factors for theoretical determinations performed with different theory levels. On these bases, optimization was carried out using a non-gradient based, mono-objective, Evolutionary Algorithm (EA) in OptiSMOKE+ [62], capable of handling all the parameters as uniformly distributed random variable within their estimated bounds, simultaneously.

The manuscript is organized as follows. Section 2 presents the proposed methodology. Section 3 describes the results, for pure ammonia on a wide range of experimental conditions covering ignition delay times in Shock Tubes (ST) and Rapid Compression Machines (RCM), Plug Flow (PFR) and Jet-Stirred Reactors (JSR) speciation measurements and laminar burning speed in Freely Propagating Flames (FPF). Finally, conclusions are presented in Section 4.

2. Methodology

2.1. Optimization procedure

As in [18],[20], all the parameters of the selected rate constants expressed according to the modified Arrhenius expression ($k = A\ T^{\beta}\ \exp(-E_a/RT)$) undergo optimization, i.e. pre-exponential factors (A), temperature exponents (β), and activation energies (E_a). The logarithmic expression of the rate constant adopted in this work yields:

$$\kappa = \ln(k(T)) = \ln(A^*) + \beta \ln\left(\frac{T}{T_{ref}}\right) - \frac{E_a}{R}\left(\frac{1}{T} - \frac{1}{T_{ref}}\right)$$
$$= \alpha^* + \beta \ln\left(\frac{T}{T_{ref}}\right) - \varepsilon\left(\frac{1}{T} - \frac{1}{T_{ref}}\right) \quad (1)$$

where, α^*, β, and ε are continuous random variables representing the Arrhenius parameters, usually assumed to be uniformly [59] or normally [63] distributed. In Eq. (1), A^* is a re-parametrized form of the pre-exponential factor at the reference temperature T_{ref}:

$$A^* = A\ T_{ref}^{\beta} \exp\left(-\frac{\varepsilon}{T_{ref}}\right), \quad (2)$$

The re-parametrization in Eq. (2) minimizes the high correlation between the parameters of the Arrhenius equation, and makes parameters estimation easier [64],[65]. In this work, a reference temperature of 1000 K was adopted for all reactions.

The uncertainty of the rate coefficients is usually assumed as symmetric, and is reported in literature in terms of f_r factor [15], being defined as follows:

$$f_r = \frac{\kappa_{max} - \kappa_0}{\ln(10)} = \frac{\kappa_0 - \kappa_{min}}{\ln(10)}, \quad (3)$$

The problem of defining the constraints for the active parameters was dealt with in several studies. In the deterministic framework of B2B-DC [27],[30], the feasible set is obtained by combining the initial bounds of both active variables and experimental data. In MUM-PCE [43], a statistical approach is adopted, which assumes "a priori" distributions for both the model parameters and the measurements, and produces "a posteriori" distributions for both

model parameters and predictions. These two approaches were recently compared, and they were found to give consistent results [32]. Nagy and Turányi [66],[67] considered the dependence of f_r on temperature, and proposed a method to determine the covariance matrix and the multivariate normal distribution of the transformed Arrhenius parameters from prior information on the rate constant. In a later study, Nagy et al. [68] recommended the adoption of temperature-independent uncertainty and uniform distributions for Arrhenius parameters in case of little prior information. As we discuss later (see 2.5), the nominal mechanism in this study largely relies on ab-initio calculations. For this reason, the temperature dependence of f_r is not accounted for, and uniform distributions for all the active variables are employed.

As reported in Eq. (1), κ is a weighted sum of three random variables with joint uniform distribution, which results in a higher probability near κ_o [68]. For the sake of simplicity, in the following we assume that for all temperatures the kinetic constant κ is a normally distributed random variable with mean value κ_0, corresponding to $\kappa(\mathrm{p_o})$, and standard deviation σ_κ, with $\boldsymbol{p_0} = [\alpha_0, \beta_0, \varepsilon_0]$. As in [43],[59], we assume that f_r corresponds to the $2\sigma_\kappa$ of the distribution of κ, and we constrain it at 3σ. From Eq. (3), $\kappa_{\max}$ and $\kappa_{\min}$ can be obtained, i.e. the maximum and minimum linear constraints of κ in T∈[T_{min}, T_{max}]. As an element κ_i in κ can be retrieved by sampling from the distributions of the normalized Arrhenius parameters, f_r can also be propagated from κ to α, β, and ε to estimate their bounds. In the following, the hypothesis of mutual independence between parameters is used exclusively to achieve this goal. Given the equation:

$$10^{f_r} = \frac{k_{\max}(T)}{k_0(T)} = \frac{k_0(T)}{k_{\min}(T)} = \exp\left[\Delta\alpha + \Delta\beta \ln(T) - \Delta\varepsilon T^{-1}\right], \quad (4)$$

and assuming that the maximum variation Δp_i of one parameter is determined by projecting the uncertainty of κ on the parameter itself (i.e. keeping constant the other two to their nominal values so that $\Delta p_i = 0$), the following constraints can be retrieved:

$$\alpha_0 - \ln\left(10^{f_r}\right) \le \alpha \le \alpha_0 + \ln\left(10^{f_r}\right), \quad (5)$$

$$\beta_0 - \frac{f_r}{\log_{10}(T)} \le \beta \le \beta_0 + \frac{f_r}{\log_{10}(T)}, \quad (6)$$

$$\varepsilon_0 - T f_r ln(10) \le \varepsilon \le \varepsilon_0 + T f_r ln(10), \quad (7)$$

This operation results in 2 non-linear constraints for β and ε in T∈[T_{min}, T_{max}]. However, it can be shown that:

$$\lim_{T\to\infty} k(T) = \exp(\alpha) T^{\beta} \quad (8)$$

$$\lim_{T\to 0} k(T) = \exp\left(-\varepsilon T^{-1}\right) \quad (9)$$

The limits (8) and (9) indicate that at high temperature, the term T^β controls the value of κ, while the contribution of εT^{-1} is progressively smaller. The opposite is true for low temperatures. Thus, the sensitivity of κ to β is maximum at T_{max}. Conversely, the sensitivity of κ to ε is maximum at T_{min}. By bounding β and ε in Eqs. (6) and (7) at T_{max} and T_{min}, respectively, we ensure that $\kappa(\alpha_0, \beta_{max}, \varepsilon_0, T)$, $\kappa(\alpha_0, \beta_{min}, \varepsilon_0, T)$, $\kappa(\alpha_0, \beta_0, \varepsilon_{max}, T)$, and $\kappa(\alpha_0, \beta_0, \varepsilon_{min}, T)$ never violate the linear constraints on $\kappa(T)$, when T∈[T_{min}, T_{max}]. In this work, the minimum and maximum temperatures are 300 and 3000 K, respectively. Indeed, from the definition of f_r in Eq. (3), also $\kappa(\alpha_{max}, \beta_0, \varepsilon_0, T)$, and $\kappa(\alpha_{min}, \beta_0, \varepsilon_0, T)$ do not violate the mentioned constraints. The adoption of this methodology for the estimation of parameter boundaries has two main advantages. First, it reduces the probability of sampling a kinetic rate constant $\kappa(T)$, which violates the above mentioned linear constraints, with respect to previously proposed methods [69]. Further details about this feature are provided in the Supplementary Material (SM). Secondly, it enables the optimization of PLOG-based reactions. As an example, Fig. 1 shows the projections of the parameters bounds on the kinetic constants of the reaction NH_2+NO_2=H_2NO+NO. Those resulting from varying only α overlap with the 2σ of the distribution of κ. On the other hand, those resulting from the variation of β and ε overlap with the 2σ of k only at T_{max} and T_{min}, respectively, while not exceeding them along T∈[T_{min}, T_{max}]. The limit values of the corresponding κ distribution, i.e. $\kappa(\alpha_{max}, \beta_{max}, \varepsilon_{min})$ and $\kappa(\alpha_{min}, \beta_{min}, \varepsilon_{max})$, are also displayed. They include the entire space of κ and exceed it. In fact, since the parameters are correlated [66], not all the combinations of the three are valid.

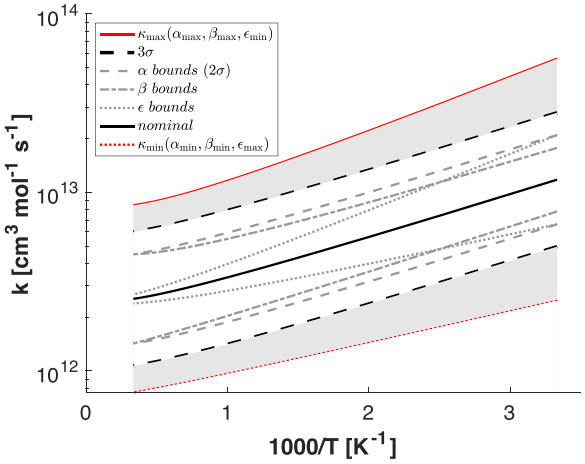

Fig. 1. Reaction rate constant k as a function of parameters bounds for NH_2+NO_2=H_2NO+NO [98].

All the combinations, which result in values of κ belonging to the area between the limit values and the 3σ bounds of the distribution of κ, are excluded from the set of eligible parameter combinations. This is achieved by introducing a penalty function during the optimization: the associated objective function is equal to curve matching index of 0 (i.e. the maximum error in the CM methodology). Conversely, for each valid combination suggested by the adopted optimization algorithm, a corresponding set of simulations responses are obtained by performing model evaluations for the entire database. Subsequently, the CM indices:

$$CM_j = \frac{\left(d^0_{j,L_2} + d^1_{j,L_2} + d^0_{j,p} + d^1_{j,p}\right)}{4} \in [0,\ 1], \quad (10)$$

are calculated, as a weighted sum of 4 dissimilarity indices, for each dataset j. A unitary CM value indicates a perfect matching between model evaluations and experiments. In particular, functional estimations of both experimental, *g(x)*, and model evaluations, *m(x)* (and their derivatives *g'(x)* and *m'(x)*) are obtained by interpolating smoothed splines, which result in satisfactory approximations of both data points and first derivatives [60],[61]. Based on these estimations, the dissimilarity indices are computed as follows:

$$d^0_{j,L_2} = \frac{1}{1 + \frac{\|m-g\|}{|D|}} \in [0,\ 1], \quad (11)$$

$$d^1_{j,L_2} = \frac{1}{1 + \frac{\|m'-g'\|}{|D|}} \in [0,\ 1], \quad (12)$$

$$d^0_{j,p} = 1 - \frac{1}{2}\left\| \frac{m}{\|m\|} - \frac{g}{\|g\|} \right\| \in [0,\ 1], \quad (13)$$

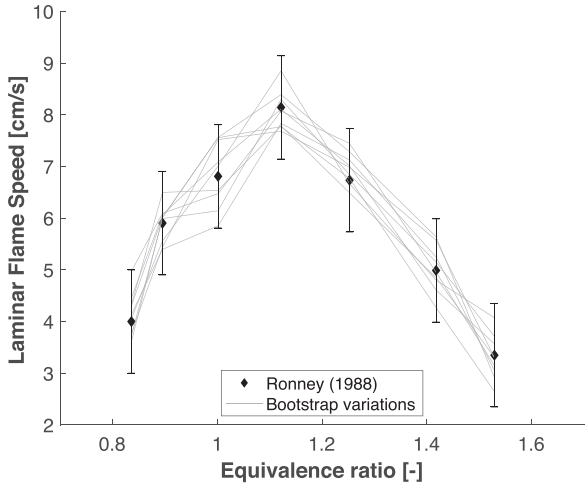

Fig. 2. Example of bootstrap procedure with 10 variations. Experimental data from [83].

$$d^1_{j,p} = 1 - \frac{1}{2}\left\| \frac{m'}{\|m'\|} - \frac{g'}{\|g'\|} \right\| \in [0,\ 1], \tag{14}$$

where $|D|$ is the intersection of the domain between g and m. For instance, if the abscissa values of g belong to [500,1500], and those of m belong to [400, 1800], the value of $|D|$ would be 1000 (i.e. $|D|$ =1500–500). The $\|g\|$ is the L_2-norm of the function g. All the dissimilarity indices are intrinsically constrained between 0 and 1, where 1 indicates maximum similarity, and 0 maximum dissimilarity. Individually, d^0_{j,L_2} depends on the area enclosed by g and m, while d^1_{j,L_2} evaluates the same quantity between their respective derivatives. Hence, the first generalizes a classical L_2-norm, while the second extends it. On the other side, the Pearson dissimilarity measures $d^0_{j,p}$ and $d^1_{j,p}$ indicate perfect matching if g and m, and their derivatives, only differ by vertical translation. Further mathematical details and examples are given in [60],[61]. In order to account for the uncertainty in the evaluation of (10), a bootstrapping procedure [70] on the experimental data is carried out. This procedure relies on the assumption that each data point is normally distributed within its experimental uncertainty. A sufficiently large set of possible experimental trends is generated taking random samples from the above-mentioned distributions. Fig. 2 displays an example of the application of the bootstrap procedure for laminar flame speed data, where 7 gaussian distributions (i.e. one for each data point) were sampled 10 times to generate as many bootstrap variations.

A set of 50 bootstrap variations (N_b=50) for each data point was adopted after verifying the substantial independence of the final output on a further broadening of the set. Thus, the objective function in this work is defined as:

$$M = \frac{1}{DS}\sum_{i=1}^{DS}\left[1 - \frac{1}{N_b}\sum_{j=1}^{N_b}\left(CM_j\right)\right]_i, \tag{15}$$

Where, DS is the number of target datasets and N_b is the number of bootstrap variations. In order to discuss its advantages, the final index (Eq. (15)) is compared to the modified versions of L_1-norm and L_2-norm:

$$L_1 = \frac{1}{DS}\sum_{i=1}^{DS}\frac{1}{E_i}\sum_{j=0}^{E_i}\left|\frac{Y^{\exp}_{i,j} - Y^{sim}_{i,j}}{\sigma\left(Y^{\exp}_{i,j}\right)}\right|, \tag{16a}$$

$$L_2 = \frac{1}{DS}\sum_{i=1}^{DS}\frac{1}{E_i}\sum_{j=0}^{E_i}\frac{\left(Y^{\exp}_{i,j} - Y^{sim}_{i,j}\right)^2}{\sigma^2\left(Y^{\exp}_{i,j}\right)}, \tag{16b}$$

where E_i is the number of discrete experiments belonging to the i^{th} dataset. Y_{ij}^{exp}, Y_{ij}^{sim} and σ are the values of the j^{th} measurement, simulation, and experimental uncertainty in the i^{th} dataset, respectively.

As in Olm et al. [71], when the error on ignition delay times is evaluated, the following transformation is used, Y_{ij}^{exp}=ln(y_{ij}^{exp}) and Y_{ij}^{sim}=ln(y_{ij}^{sim}), where the y_{ij}^{exp} and y_{ij}^{sim} refers to the absolute experimental and simulated values, respectively. For other experimental targets, such as species concentrations and laminar flame speeds, the logarithmic transformation is not used. The same is done for the estimation of Curve Matching indices for ignition delay times.

In this work, the objective function minimization is performed by means of an Evolutionary Algorithm (EA) [72], whose solution is less dependent on the initial guess compared to other algorithms [35]. Indeed, in EA the initial guess is a set of sampled combinations of active parameters, i.e. the 'population'. Initially, a population of 100 different combinations of parameters is sampled, evaluated and labelled with objective function values. Then, the algorithm starts the first iteration (a *'generation'*), where the elements of the current population (the *'parents'*) are ranked applying a linear scaling of probability based on the corresponding objective function values. In general, the best performing parents undergo uniform crossover, where a couple of parents (or a *'chromosome'*) is selected, and each parameter value can be swapped between the two with a probability equal to the crossover rate p_c. This operation produces a new pair of elements (the '*off-springs*'), resulting from the cross-over of as many *parents*. Subsequently, mutation is introduced. In particular, for each new *off-spring*, every variable has the same probability to mutate, according to the mutation rate p_m. A non-uniform mutation operator was adopted to assign a new parameter value by sampling from its distribution. When mutation and cross-over are complete, a resulting population of 200 is obtained, i.e. twice the size of the initial one. In this work, a replacement strategy, which selects the 50 best individuals in 200 elements, and randomly selects other 50 from the remaining 150, was adopted. This ensures the balance between global and local search. The adopted probability of cross-over (p_c=0.65) and mutation (p_m=0.5) were suggested by Elliott et al. [35]. The new parent population undergoes the same procedure iteratively until satisfactory accuracy is achieved. In the present work, Dakota [72] and OpenSMOKE++ [73],[74], are coupled in OptiSMOKE++ [62] to perform the optimization. The first toolbox is specifically conceived to address engineering problems such as optimization, calibration and uncertainty quantification. On the other hand, OpenSMOKE++ enables the simulation of multiple experimental combustion facilities typically considered for kinetic model development and validation.

2.2. Optimization of reactions in PLOG formalism

For those reactions exhibiting a "fall-off" behaviour, the rate *k(T,P)* is usually determined from the low and high-pressure limit constants, together with a blending function that smoothly connects the limiting rates across the fall-off regime, using different possible formulations. Among these, the Troe formulation [75],[76] is the most widely used. An alternative formulation based on logarithmic interpolations, expressed with the so-called PLOG, has been recently proposed [46], and is rapidly growing in popularity because of the potentially superior accuracy, thus becoming the new standard formalism. PLOG reactions are typically introduced

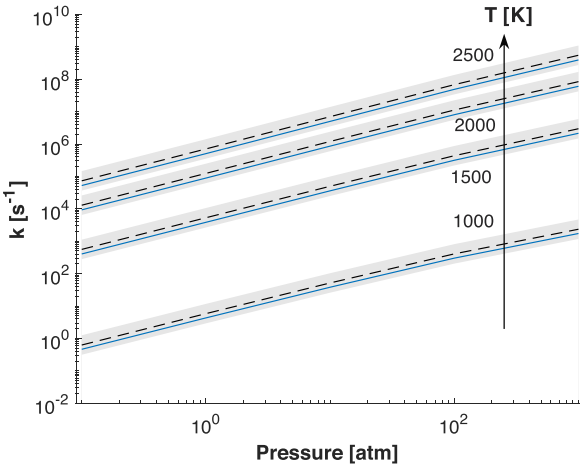

Fig. 3. 3D behaviour of a PLOG reaction. R143: HNO=H+NO before (dashed line) and after optimization (continuous line).

in a kinetic mechanism using multiple Arrhenius rate constants accounting for temperature dependence at constant pressures covering the entire range of conditions from the low to the high-pressure limits. Then, a proper (i.e. logarithmic) interpolation is adopted for the intermediate pressures. In this way, the combined effects of pressure (P) and temperature (T) on the rate constant k is properly accounted for. As a result, the three Arrhenius parameters for each pressure value cannot be optimized independently from each other, even within their own uncertainty ranges, in order to keep the physical consistency in the whole pressure domain. On the contrary, the same optimization performed using all the nominal pre-exponential factors, temperature exponents and activation energies, i.e. treating reactions at different pressures as independent from each other, would result in a non-monotonic behaviour with arguable physical meaning. Additionally, since the number of reactions within the same PLOG is the result of a fitting needed to describe complex k(T, P) with a small acceptable error, the number of parameters to be handled scales accordingly. This may result in an abrupt increase in the number of parameters for a single reaction. For the first time in literature, we propose an approach to optimize the parameters at all pressures simultaneously, based on what proposed for the parameters bounds in the previous section, using only three, uniformly distributed random variables with an average value of 0, and constrained in the following ranges:

$$X_1 \in \left[-\ln\left(10^{f_r}\right), \ln\left(10^{f_r}\right)\right], \tag{17}$$

$$X_2 \in \left[-\frac{f_r}{\log_{10}(T_{\max})}, +\frac{f_r}{\log_{10}(T_{\max})}\right], \tag{18}$$

$$X_3 \in [-f_r T_{\min} \ln(10), +f_r T_{\min} \ln(10)], \tag{19}$$

These variables are associated with α, β, and ε, at all pressures, respectively. The value of X_1 is sampled from its distribution and added to all the α, at different pressures, i.e. each reaction rate is changed by the same factor, and the same is done for β_0 and ε_0, using X_2 and X_3. As an example, Fig. 3 displays results from the Section 3 about the comparison between nominal and optimized rate for the decomposition reaction HNO=H+NO, to which we attributed an uncertainty factor f_r of 0.3. The reported pressure values for this reaction are 0.1,1,10,100 and 1000 bar. Fig. 3 highlights the preserved consistency in the pressure dependent behaviour of the reaction rates at different temperatures.

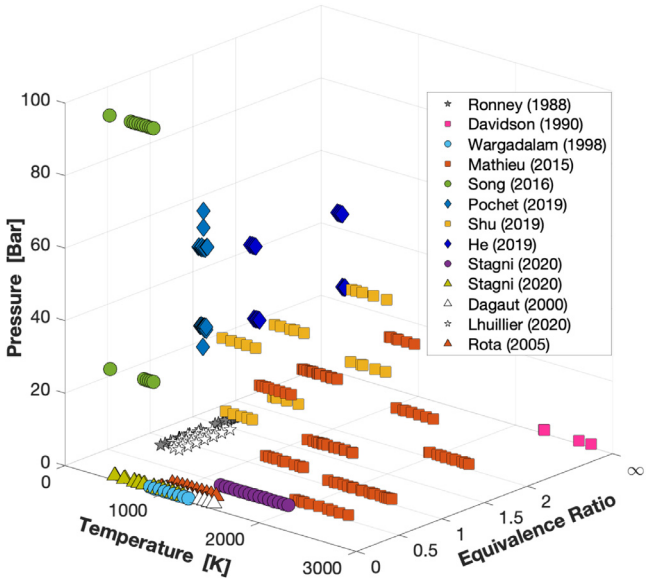

Fig. 4. Collected experimental data on Ammonia combustion in terms of operating conditions (temperature, pressure, and composition).

2.3. Database

Fig. 4 summarizes the features of each test case (TC) in the temperature, pressure and composition space. The experimental data considered in this work cover the entire space of operating conditions.

The database, consisting of 60 different datasets (with 635 experimental points) from different test cases, was divided in optimization and validation targets (i.e. 75% and 25%, respectively). For high-temperature conditions, the shock tube experiments from Mathieu and Petersen [55], and Shu et al. [77] cover ignition delay time in a wide range of composition (ϕ = 0.5–2.0) and pressures (10–40 bar). Stagni et al. [20] reported data for ammonia oxidation close to the atmospheric pressure for lean mixtures in two different systems, namely jet stirred and flow reactors. At low temperatures, He et al. [78] and Pochet et al. [79] provided auto-ignition data at higher pressures, for lean, stoichiometric and rich mixtures in rapid compression machines. Wargadalam et al. [80] and Song et al. [81] published speciation data for very lean conditions, at pressures of 1, 30 and 100 bar, in flow reactors. Davidson et al. [82] investigated ammonia pyrolysis in a shock tube at extremely high temperatures (T > 2500 K). The laminar burning speed experiments by Lhuillier et al. [51] were only considered for validation. However, flame speed targets were included by using the data from Ronney [83]. The TCs from Rota [84] and Dagaut [85] in jet stirred reactors were excluded from the optimisation set, yet used for validation, as they cover a part of the operating conditions space which is already densely populated (see Fig. 4).

2.3.1. Numerical simulations

In this work, the ignition delay time was calculated using the definition reported in the corresponding experimental paper. The constant volume assumption was used to simulate the shock tube data of Mathieu and Petersen [55], and Davidson [82]. In reproducing the data from Shu et al. [77], gas dynamic effects were accounted for using the methodology described in [86]. The RCM data were reproduced under the hypothesis of adiabatic core [87], and detailed volume profiles from He [78] and Pochet [79] were used to properly account for the compression stroke and heat exchange effects in each experiment. For the flow reactor experi-

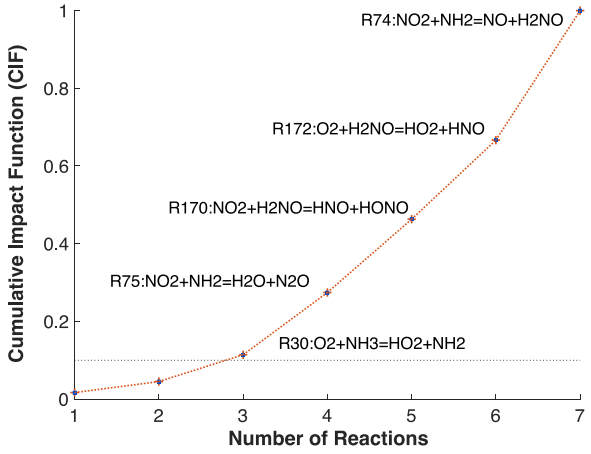

Fig. 5. Example of reaction selection using the Cumulative Impact Function (CIF) for the test case from Song [81]. The horizontal line represents the chosen threshold of 90% of the impact.

ments from Stagni et al. [20], measured, non-reactive temperature profiles were given as input to the simulations.

2.4. Impact-based reactions selection

Warnatz [88] suggested the joined use of sensitivity and uncertainty to identify key reactions in a detailed kinetic mechanism. This concept was also used in optimization of kinetic models for the first time by Frenklach et al. [25], who selected the active variables using a ranking based on the "impact factor", i.e. considering the absolute values of sensitivity coefficients multiplied by their own uncertainty. Later on, this index was also referred to as "sensitivity-uncertainty index" [89] and "optimization potential" [45].

In this work, parameters selection is performed separately for each Test Case (TC), in order to retain all the important elementary steps. First, a local sensitivity analysis [73], was performed for each experimental point in TC. This produces a vector S containing the average normalized sensitivity coefficient s_r (Eq. (20)) for each reaction $r \in R$.

$$s_r = \frac{1}{\boldsymbol{D}} \sum_{d=1}^{\boldsymbol{D}} \left| \frac{A_r}{Y_{ref}} \frac{\partial Y_d}{\partial A_r} \right|, \tag{20}$$

where A_r is the pre-exponential factor of the reaction r, Y is the optimization target, Y_{ref} is a normalizing factor, and D is the number of experiments for the test case. This vector is then sorted and elaborated in a cumulative sum, and the resulting one is referred to as *Cumulative Sensitivity Function* (CSF). This methodology allows exploiting the properties of the cumulative sum, which enables the selection of reactions to be optimized with proper priority. In particular, a subset of sensitive reactions S_S can be retrieved by establishing a threshold corresponding to a defined fraction of the sum of the 1st order sensitivity coefficients related to a specific TC. Subsequently, the test case related impact factor vector for each reaction r is evaluated with Eq. (21):

$$I_{\boldsymbol{r},\boldsymbol{s}} = s_{\boldsymbol{r},\boldsymbol{s}} \cdot f_{\boldsymbol{r}}, \tag{21}$$

where each element of the sensitivity vector is multiplied with the corresponding uncertainty factor [15],[16]. Fig. 5 shows an example of Cumulative Impact Function (CIF) obtained by applying the cumulative sum for the test case from [81]. Here only 5 reactions, are responsible of 90% of the impact. The remaining set of 196 reactions retaining ~10% of the total impact are excluded in further investigations. All selected reactions at CSF and CIF level are reported in Table S1 (SM).

2.5. Uncertainty estimation

Among the reactions included in this work 13 out of 43 rates come from experiments together with their uncertainty factors (see table S1 in SM). These reactions were selected by applying the procedure described in Section 2.4 to each experiment inside the database (Section 2.3). The remaining part involves phenomenological rate constants determined using first principle (*ab-initio*) calculations. Klippenstein et al. [18] declares that an uncertainty factor of 0.3 (see Eq. (3)) can be obtained for the rate constants of the reactions belonging to the families considered in the present work. In a more recent publication Cavallotti et al. [90] showed that the level of accuracy attainable using the *ab-initio* master equation approach can be a factor of 0.3 (see Eq. (3)) or lower. The main factors contributing to uncertainty in a rate constant calculation derive from: 1) the level of theory used to determine the energy of stationary points on the potential energy surface (PES); 2) the theoretical methods adopted for the computation of the high pressure rate constant; 3) the level at which pressure effects and reaction dynamics on a multi-well PES are described; 4) the treatment of anharmonicities, most importantly the description of torsional motions, if active for a specific reaction; 5) the availability of experimental rate constant data. The values from the protocols of Cavallotti et al. [90] and Klippenstein et al. [18] are assumed as the lower uncertainty threshold in the present work, while the remaining ones are assigned with a policy of inverse proportionality to the adopted level of theory. This threshold corresponds to a f_r factor equal to 0.3 (see Eq. (3)). The following penalty terms were used:

1) Concerning the level at which electronic structure calculations were performed, computational protocols where energies are computed at the CCSD(T)/CBS or higher have no penalty term. For CBSQB3 calculations a 0.2 factor is added to f_r, so that the uncertainty goes from 0.3 to 0.5. For DFT calculations, such as B3LYP, a factor of 0.3 is added, thus increasing the uncertainty factor to 0.6.
2) High pressure rate constants can be determined using (in order of decreasing accuracy): i) Variable Reaction Coordinate Transition State Theory (VRC-TST), ii) variational transition state theory (VTST), or iii) conventional transition state theory (TST), where TST or VTST are assumed to be suitable to study abstraction or addition reactions, while VRC-TST or VTST are necessary to study barrierless processes such as recombination or bond dissociation reactions (i.e. unimolecular initiations reactions). A penalty of 0.3 and 0.1 was assigned to TST and VTST, respectively, in case of radical/radical recombination or decomposition reactions. Otherwise, penalties of 0.1 and 0.05 were assigned.
3) Methods where the impact of pressure dependence and multi-well dynamics on the rate constant are studied using the Master equation approach coupled with TST and ab initio calculations (AI-TST-ME), are generally more accurate than methods with lower theoretical detail, such as QRRK. The adopted penalty term is 0.4, so that for QRRK methods the estimated rates are associated with an uncertainty factor ranging between 0.7 and 1. This value was adapted to 0.5 for Dean and Bozzelli [91], who also compared their rates with experimental data and adjusted their recommendations accordingly.
4) Anharmonicities can have a quite relevant impact on rate constants if torsional motions are present [92]. If no torsional motion treatment, such as the hindered rotor model, is used when torsional motions are active, a penalty term of 0.5 is added.

More details regarding the uncertainty estimations in this work are provided in the Supplementary Material. In order to further support the general validity of the optimization method, a sensitivity analysis to the assigned uncertainty parameters was carried out

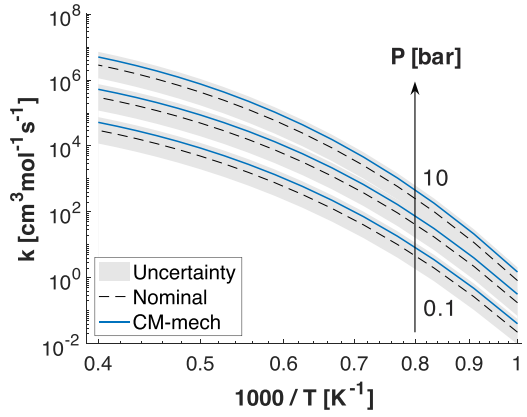

Fig. 6. Sum of reaction rates constants for R111 and R112 at different pressures.

by performing three different optimizations with a limited number of targets (see SM). The first, is carried out with uncertainty factors used in this work, the others by multiplying all of them by a factor of 0.5, and 2. Results are reported in the Supplementary Material showing that the majority of the resulting kinetic rate constants overlap with those obtained with the nominal values of f_r (Eq. (3)), thus supporting the robustness of the methodology.

3. Results and discussion

The model from Stagni et al. [20], hereafter reported as 'nominal', consists of 31 species and 210 reactions. The proposed methodology for mechanisms optimization aims at improving the nominal one considering all target datasets and uncertain parameters, simultaneously. This represents a significant difference from previously suggested approaches, where a hierarchical and systematic procedure was adopted instead [41]. As already explained in Section 2.3, the 60 datasets within the database were split into two parts, i.e. optimization and validation targets (45 and 15, respectively) to evaluate *a-posteriori*the loss in predictability on the datasets, which were not used in the optimization. The evaluation of the impact of different objective functions on the optimized model performance is the main purpose of this work. Using the same database, three detailed kinetic mechanisms were obtained using CM (Eq. (15)), L_1-norm (Eq. (16a)), and L_2-norm (Eq. (16b)). These are hereafter referred to as CM-mech, L_1-mech, and L_2-mech, respectively. Specifically, CM-mech is available in the Supplemental Material. The thermodynamic and transport properties (which were not involved in the optimization) were taken from [20].

The reactions to be optimized were selected using a cumulative sensitivity threshold (see 2.4) equal to 90%, applied for each test case, leading to a sensitive subset of 41 reactions. Then, a selected subset of 24 most impactful reactions was obtained using the same threshold on the CIF (see 2.4) after the estimation of reaction rates uncertainties (see Section 2.5). More details about which reactions were included in this sub-set are given in SM. It is also important to mention that 4 out of 24 reactions (namely (R24, R111 and R112, and R143) are expressed with PLOG formalism. Indeed, R111 and R112 are duplicate of the same reaction, as evaluated by Dean and Bozzelli [91].

$$NH_3 = NH_2 + H \quad \text{(R24)}$$

$$N_2H_2 = NNH + H \quad \text{(R111)}$$

$$HNO = NO + H \quad \text{(R143)}$$

Overall, optimization was carried out considering 68 active variables. Nonetheless, only 56 out of 68 are directly linked to one single Arrhenius parameter, in pressure-independent reactions. Due to the nature of the four pressure-dependent reactions (i.e. PLOG), the remaining 12 uncertain parameters correspond to 45 Arrhenius parameters in the kinetic mechanism (see Section 2.2). Subsequently, 101 kinetic parameters were optimized simultaneously.

Fig. 6 shows a comparison between the optimized duplicate PLOG using the CM as objective function, and the nominal reaction. The former falls within the 2σ uncertainty band and it is increased by the same factor, for all pressures.

On average, the optimized rate deviates from the nominal value by +76.4% at the low-pressure limit and by +78.2% at the high-pressure limit, due to the sum of R111 and R112 at different pressures. The pre-exponential factors at three different pressures were optimized by multiplying them by a factor of ~1.567 and ~1.221, for R111 and R112, respectively. Regarding other parameters, for R111 the temperature exponent is kept constant, while it increases for the R112 by a factor of 0.065. Inversely, a more significant change of −315.7 [cal/mol] in the energies of activation for R111, and no variation for the same parameter in R112, was observed.

The agreement with the laminar flow reactor experiments from Stagni [20] is mostly affected by reactions R24, R111, R112, and R143. Remarkable results are obtained, with all objective functions, for predictions of O_2 consumption, NH_3 conversion, H_2O and NO formation, as highlighted in Fig. 7. The major change occurs at 1523 K for NO, where also ammonia, oxygen, and water are significantly affected in shape. At this temperature, NH_3 consumption is delayed and NO volume fraction decreases by one order of magnitude (from ~1.3 to ~0.2 v/v%), resulting in a largely improved agreement with the experimental data for both CM-mech and L_2-mech, while the L_1-mech slightly underestimates the concentration of NO at this point. For temperatures between 1600 and 1800 K, none of the models can reliably reproduce the experimental observations. For the temperature ranges [1523,1600] and [1800,2000] K, the L_2-mech shows the best agreement with the experiments. For NO formation, the CM index (see Eq. (10)) increases from 0.849 to ~0.9 for all the optimized mechanism. The L_2-norm for this dataset decreases from ~1560 to 172, 160 and 158 for CM-mech, L_1-mech and L_2-mech, respectively.

In order to discuss this case further, sensitivity and rate of production analysis of both nominal and CM-mech were performed at 1523 K to explain how modifying kinetic rate constants led to the improvement discussed above. Figure 8a shows the main sensitive reactions for the formation of NO. R26 is characterized by a negative sensitivity coefficient, which relatively increases after optimization. This happens because the rate constant for this reaction increases by a factor of ~2, as shown in Fig. 8b, and strongly impacts ammonia conversion, as well as NO formation. Existing direct measurements for R26 [93],[94] reported a lower rate with respect to the nominal mechanism. Therefore, model optimization and measurements seem to recommend conflicting rate modification for this reaction. However, recent advanced theoretical calculations [95] reported an increased rate for R26 with respect to the nominal one, in agreement with the optimizer. In this context, a better characterization for this reaction is recommended for future mechanism development. For instance, new experiments may be carried out to confirm previous findings [95].

Globally, the rate of NH_3 consumption in the optimized mechanism decreases because of the competition between R26 and R27.

$$NH_3 + H = NH_2 + H_2 \quad \text{(R26)}$$

$$NH_3 + OH = NH_2 + H_2O \quad \text{(R27)}$$

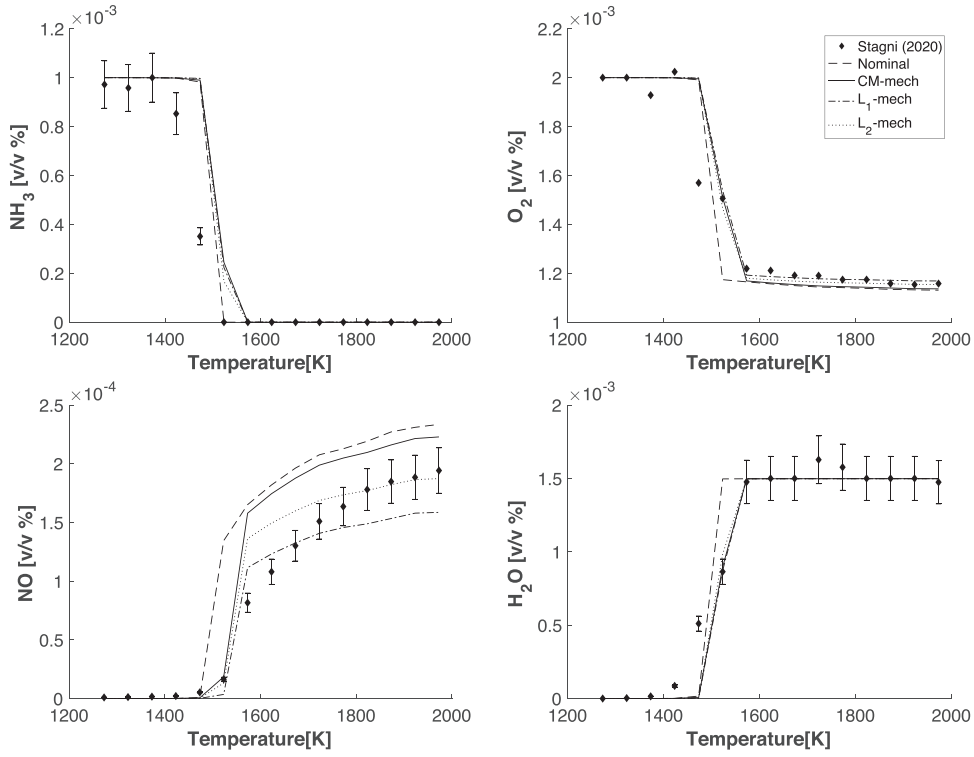

Fig. 7. Comparison between predictions of outlet molar fraction of NH_3, O_2, NO and H_2O with nominal and optimized mechanism for a lean NH_3/O_2 mixture in a flow reactor, at 1.25 bar. Experimental data from [20].

NH_2 is formed in a lower amount, since R27 is the dominant kinetic step for its formation. This explains modified trend for ammonia in Fig. 7. In spite of the ~27% increase in the combined kinetic rate constant of R31 and R32 (see Fig. 8c), the rate of production for HNO decreases due to the limited availability of NH_2. It is clear that in L_2/L_1-mech the reduced production of HNO is enhanced by a decrease in R31 and R32.

$$NH_2 + O = HNO + H \quad \text{(R31)}$$

As reported by Stagni et al. [20], HNO plays a key role in NO_x formation. This species dissociates through R143, and undergoes H-abstraction in R144, forming nitrogen-oxide (NO).

$$HNO = NO + H \quad \text{(R143)}$$

$$H + HNO = NO + H_2 \quad \text{(R144)}$$

As shown in Fig. 8a, R143 and R144 exhibit positive and negative sensitivity coefficients, respectively. Therefore, the reduction of R143 by a factor of ~2 (see Fig. 3) along with the increase of R144 by a factor of ~2.5 (shown in Fig. 8f) cause the pronounced NO reduction at 1523 K.

Fig. 8e shows a 6% increase in k(T) for R76, which carries an enhanced negative sensitivity coefficient in the optimized mechanism. Therefore, NO reduction is also due to its conversion to final products through such reaction.

$$NO + NH_2 = N_2 + H_2O \quad \text{(R76)}$$

Also, an average 7% increase in R39 (see Fig. 8d), along with the abovementioned deviation of R111/R112 from the nominal values, displayed in Fig. 6, strengthen the following path $NH \rightarrow N_2H_2 \rightarrow NNH \rightarrow N_2$, which bypasses NO formation during ammonia oxidation, contributing to its reduction.

$$NH + NH_2 = N_2H_2 + H \quad \text{(R39)}$$

Fig. 8d also shows the rate constants obtained in L_2/L_1-mech, which are significantly higher than those of CM-mech. This reaction, together with R31 and R32, is responsible for the difference between the three optimized mechanisms in terms of NO formation.

All the reactions discussed above were found to be impactful for laminar flame speed cases. The dataset from Ronney [83] was considered as a target in the optimization process, as measurements have been obtained in microgravity, where buoyancy does not affect the measurements. Indeed, this physical phenomenon was found to cause instabilities in the flame front for low-reactive mixtures, i.e. high pressure [96], and was correlated to discrepancies between experimental data and predictions using 1D laminar flames [97], for rich conditions. Since pure ammonia exhibits a very low laminar burning speed, and the data from Lhuillier et al. [51] were not produced in microgravity conditions, they were used only for the validation.

Fig. 9a displays the comparison between the nominal, and the optimized mechanisms on data from Ronney [83]. The predictions of CM-mech mostly fall within the experimental uncertainty and is comparable to the nominal one. On the contrary, using the pointwise definitions of the objective function, namely Eqs. (16a) and (16b), resulted in a loss in predictability. For the conditions in Fig. 9a, the 4 most sensitive reactions (and their sensitivity coefficients) are $H+O_2=O+OH$ (0.804), R39 (0.196), $NO+NH_2=OH+NNH$ (0.151), and R31-R32 (−0.095). As shown in Fig. 8c and Fig. 8d, R31-R32 decrease and R39 increases in both L_2/L_1-mechanisms. Since these reactions show a negative and a positive sensitivity coefficient, respectively, they determine an increase in reactivity for L_2/L_1-mech.

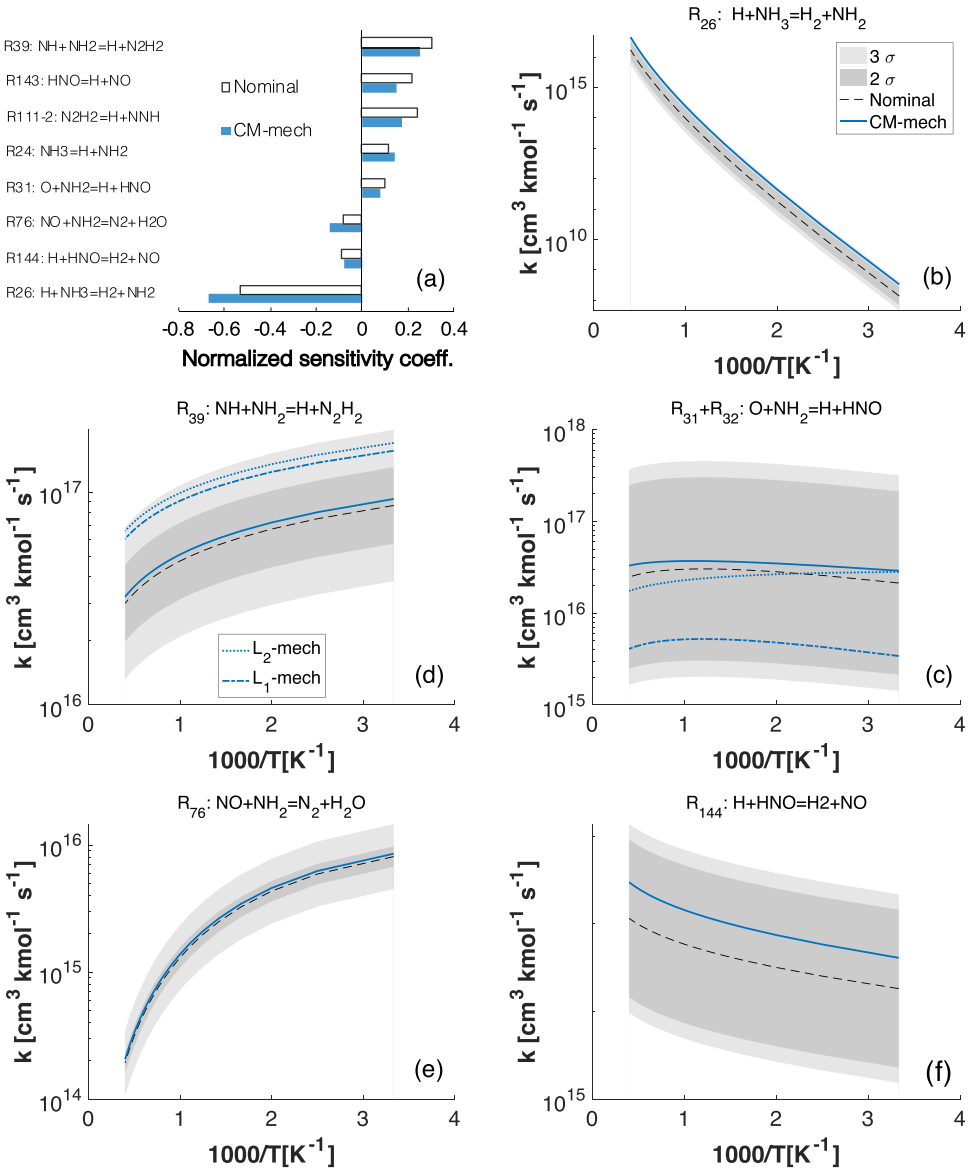

Fig. 8. Sensitivity analysis (a) and kinetic rate constants (b-f) of key reactions for NO formation at 1523 K, comparison between nominal and optimized mechanisms, in a flow reactor [20].

In particular, R39 is pushed outside the 2σ of its distribution and approaches the upper bound at 3σ for both L_2/L_1-mech, resulting in a rate with lower probability than that of CM-mech.

This reaction was found to be strongly impactful in the shock tube data from Davidson [82]. In Fig. 9b, the L_2/L_1-mech clearly outperform the nominal model, as well as the CM-mech, for the formation of NH_2 during the pyrolysis of ammonia at 2300 K and atmospheric pressure. Conversely, in the same system and operating conditions, all of the models show satisfactory agreement for the experiment on NH formation (see Fig. 9c).

Thus, to improve the predictions in Fig. 9b and the NO formation in Fig. 7 using the objective functions in Eqs. (16a) and (16b), the optimizer might force the kinetic parameters of R26 to less probable values (see Fig. 8c/d). The same does not happen CM-mech, where only 1 out of 24 reactions exceeds the 2σ. The details about kinetic rate constants of the considered reactions in optimization can be found in the supplementary material (SM).

As already discussed in [57], reactions R74 and R75 are crucial for modelling extremely lean mixtures, leading to formation of N_2O, and H_2NO. In the same study [57], R172 was defined as strongly impactful for high O_2 excess and high pressures.

$$NO_2 + NH_2 = NO + H_2NO \quad \text{(R74)}$$

$$NO_2 + NH_2 = H_2O + N_2O \quad \text{(R75)}$$

$$H_2NO + O_2 = HO_2 + HNO \quad \text{(R172)}$$

In this work, the same three reactions were found to be strongly impactful for ignition delay time predictions at high pressure in both shock tube [77] and rapid compression machine [78] experiments.

Figure 10 shows examples from the 6 ignition delay time datasets from Shu et al. [77], at high pressure. For this test case, CM-mech has the highest similarity with experiments, in fact the average CM value is 0.954, while the nominal one is 0.945. Even

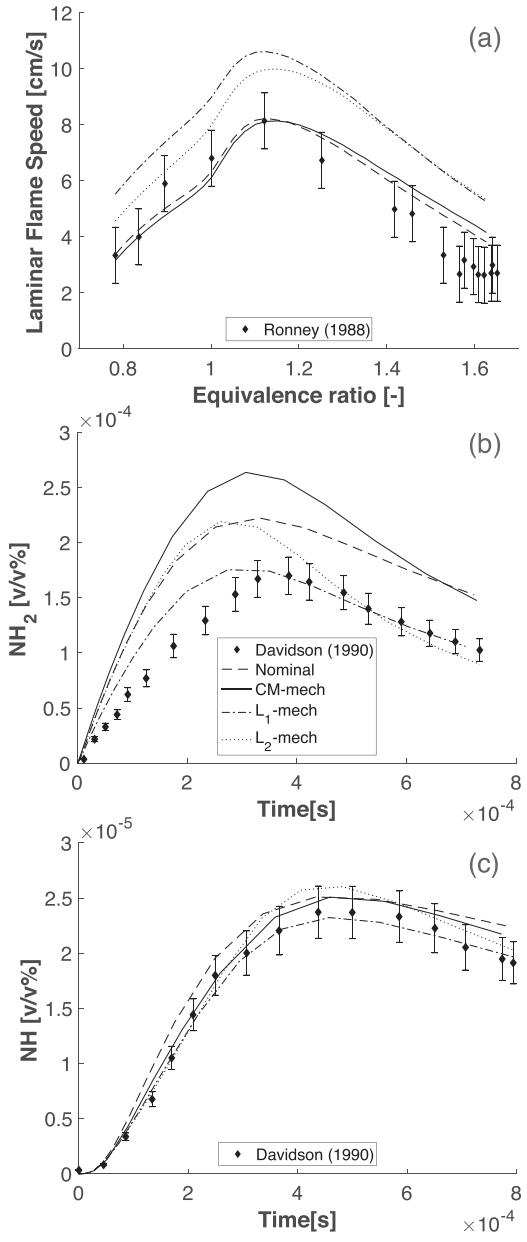

Fig. 9. Comparison of nominal and optimized mechanisms. (a) Laminar flame speed of NH_3/air mixtures in microgravity conditions at 300 K; (b) Molar fraction of NH_2 in a shock tube at 1.028 atm and 2301 K. (c) Molar fraction of NH in a shock tube at 0.986 atm and 2294 K. Experimental data from [82],[83].

though L_1/L_2-mech yield very good agreement with this test case, their curve matching indices decreases to 0.927 and 0.931, respectively. At 20 bar and in rich conditions, none of the mechanism is consistent with the experimental uncertainty at low temperatures. These results suggests that, only for these three points, measurement uncertainty might be higher than 20%.

The reactions R74, R75 and R172 were also selected for the JSR data by Stagni [20], the RCM data by Pochet [79], and the PFR data from Wargadalam [80], and Song [81]. In a similar temperature regime, ignition delay time measured at high pressures (20 and 40 bar) [78] give the most satisfying results in this work. In general, overall improvement can be appreciated in Fig. 11.

Table 1 shows the overall objective function values for the optimized models and their deviations from those of the nominal mechanism. As expected, both L1-mech and L2-mech outperform the nominal mechanism in terms of L1 and L2-norms, but the first is characterized by a lower CM index (i.e. higher 1-CM), and the second shows little improvements. This indicates that using the objectives functions 16a/16b on large databases, may lead to a lower CM index (i.e. lower agreement with experimental data) with respect to the initial model. On the other hand, the CM-mech performs better than the nominal mechanism for all the measurements, not only in terms of CM index, which is expected, but also in terms of L_1/L_2-norm (even though its gain is much lower than that of the other two optimized mechanisms).

Overall, the deviations of the objective function values between optimized and nominal mechanisms are smaller using CM with respect to the L_1/L_2-norm. Indeed, in Eq. (15), performance gains and losses for each curve contribute equally to the average value, which is always between 0 and 1. Additionally, it is very difficult, if not impossible, for any mechanism to show no similarity, or dissimilarity with experimental data, if a large set is considered. For this reason, the possible range of values for CM is even narrower than [0,1]. In general, a well-constructed and validated kinetic model, as the one used in this work, is not expected to show outstanding global improvements in terms of curve matching. Yet, significant differences between the nominal model and the CM-mech were observed in this work when looking at single curves. To further support this, the CM index (see Eq. (10)) was computed for the optimization target datasets inside the database (i.e. 44 out of 60), for all mechanisms (i.e. nominal, CM/L_1/L_2-mech). Table 2 reports the number of *negatively*/*positively* impacted datasets in each optimized mechanism. The average, and maximum deviations from the nominal CM values are also reported. This deviation is the difference in percentage between the CM index of the nominal mechanism and of the optimized ones, and it was computed for each of the 44 optimization target datasets.

The CM-based optimization approach leads to a significantly larger number of improved datasets, with respect to point-wise based approaches. In fact, L_1-mech shows reduced performances on a number of curves almost twice as big as the number of improved ones, and L_2-mech behaves similarly. Additionally, both av-

Table 1
Comparison of different error measures values for nominal and optimized mechanisms considering data used in optimization.

Mech. Label/Objective function	1-CM(% deviation)	L1-norm(% deviation)	L2-norm(% deviation)
Stagni	0.1919	3.77	176.35
CM-mech	0.1726 (−11.17%)	3.72 (−1.46%)	136.31 (−22.70%)
L1-mech	0.1962 (+1.76%)	2.71 (−31.51%)	58.94 (−66.58%)
L2-mech	0.1903 (−1.49%)	2.54 (−35.37%)	55.60 (−68.46%)

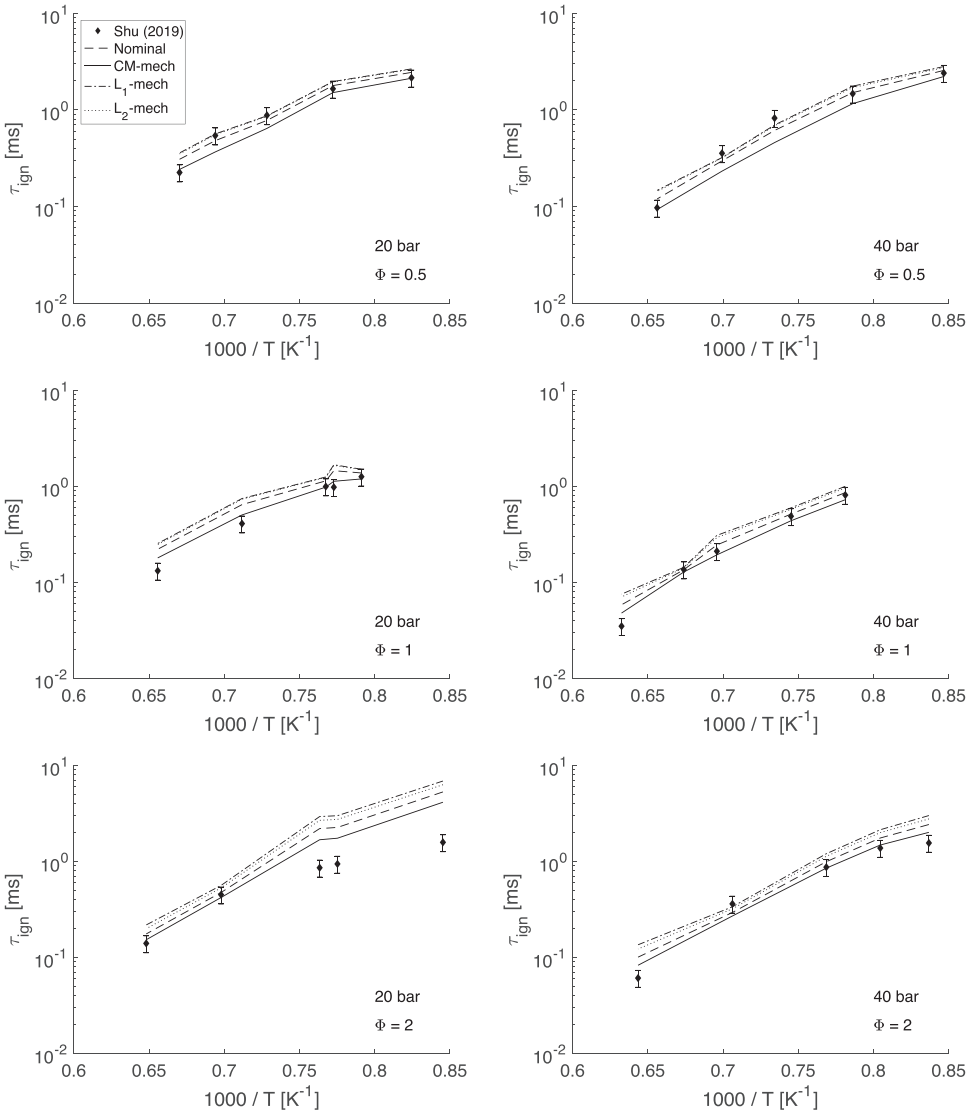

Fig. 10. Ignition delay time of NH_3/air mixtures in a shock tube for different equivalence ratios, namely 0.5,1.0, and 2.0, at elevated pressure (20 and 40 atm). Experimental data from [77].

Table 2
Performance comparisons between mechanisms on target datasets in optimization.

	Negative Impact			Positive Impact		
Adopted objective function	CM-mech	L1-mech	L2-mech	CM-mech	L1-mech	L2-mech
No. of datasets	12	26	23	32	18	21
Average CM deviation (%)	−1.42	−3.29	−3.21	+3.99	+3.29	+4.54
Maximum CM deviation (%)	−3.00	−8.75	−8.89	+14.39	+11.29	+18.35

erage and maximum negative deviations are significantly lower for the CM-mech compared to the others. For this reason, the latter approach can be considered as more conservative than the other two. Moreover, average and peak improvements in CM-mech are comparable to those of the L_2-mech, which is the one leading to the biggest local improvement. All of this is graphically summarized in Fig. 12, where the same information for the single dataset is delivered. From Fig. 12, it can be also concluded that the CM-mech yields the most homogeneous and consistent improvement over the entire subset of optimization targets even in terms of L_1 and L_2 norms.

Indeed, the absolute numerical values of relevant measures for combustion kinetic model validation (i.e. laminar burning speed, main and intermediate species concentration, and ignition delay time) range different order of magnitudes, namely from 10^{-6} to 10^{2}. As a consequence, the point-wise formulations of the objective function (i.e. Eqs. (16a and 16b)) are characterized by very different absolute values for each dataset, even when normalization is performed or the natural logarithm is adopted for the ignition delay time, as suggested by Olm [71]. Therefore, in a mono-objective optimization study targeting a wide set of experimental data, the optimizer focuses on those contributing more to the full extent of

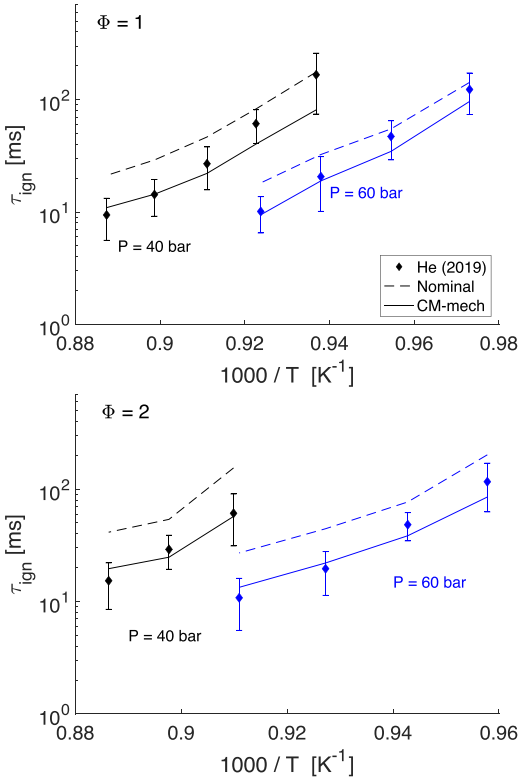

Fig. 11. Comparison between nominal and optimized mechanism for NH_3 self-ignition at pressures between 40 and 60 bar in a Rapid compression machine. Experimental data from [78].

the objective-function. CM prevents this issue, since it associates each curve with a score between 0 and 1.

4. Conclusions

In this work, we proposed a novel data-driven approach for the optimisation of detailed kinetic mechanisms. The employed optimization algorithm is the Evolutionary Algorithm (EA). For the first time the objective function was based on a recently published curve matching algorithm that is capable of quantitatively and qualitatively evaluate the agreement of kinetic models with experimental data, characterizing it in terms of L_2 norm as well as on the first derivatives and shapes of the curves. Also, a methodology to optimize the Arrhenius parameters of PLOG-based reactions was established. The interdependencies between Arrhenius expressions at different pressures were accounted for by handling three random variables for each PLOG, regardless of the number of discrete pressures specified in the mechanism. To the authors knowledge, PLOG reactions were consistently optimized for the first time within their entire temperature and pressure domain. An optimized mechanism for ammonia combustion was obtained, and it was found to outperform the initial one [20], as well as those obtained with point-wise formulations of the objective function (i.e. L_1 and L_2 norms), over a wide range of operating conditions including more than ~635 experimental data points. Addressed features of ammonia combustion were conversion, oxidation, pyrolysis, ignition and laminar flame speed in several systems. Improvements driven by optimization on all the impactful reactions were constrained to their uncertainty bounds when experiments on single elementary steps were available. For rates determined using first principles calculations, guidelines were established to estimate uncertainty ranges based on the level of theory adopted throughout the calculation protocols for electronic structures, potential energy surfaces and phenomenological reaction rate constants. In this process, 41 reactions were involved and 24 were finally selected as the most impactful by introducing a Cumulative Sensitivity Function (CSF) and a Cumulative Impact Function (CIF) for each test case in the database. As a result, the approach involved all 101 kinetic parameters, which were addressed contemporarily by the optimizer during the optimum search. Finally, the comparison between nominal and optimized mechanisms was exploited to highlight crucial reaction pathways, in need of further characterization, demonstrating the applicability of the proposed methodology as a useful tool for a more accurate evaluation of crucial kinetic constants and for design of experiments.

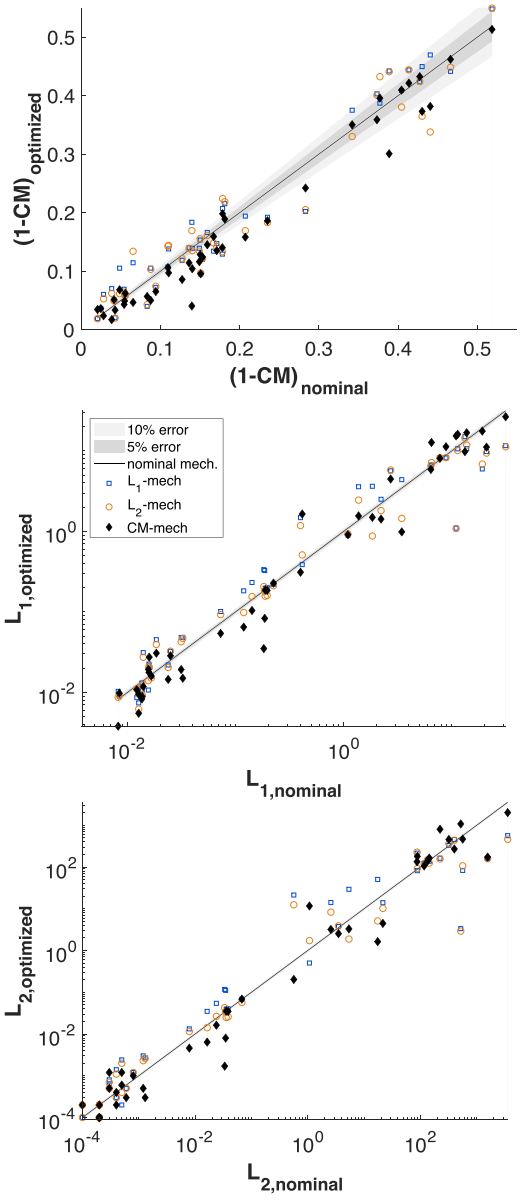

Fig. 12. nParity plot: optimized vs nominal [20] mechanisms performance for each considered dataset using error measures adopted in this work, namely curve matching, L_1 and L_2 norms.

Declaration of Competing Interest

The authors declare that they have no known competing financial interests or personal relationships that could have appeared to influence the work reported in this paper.

Acknowledgments

The authors acknowledge Luna Pratali Maffei for fruitful discussions on uncertainty of first principle calculations. The first Author acknowledges the support of Funds pour la Recherche Scientifique (FNRS) through a FRIA fellowship of the project "HOPTIMAL: Hierarchical development of OPTimised kinetic Mechanisms for Advanced combustion technoLogies". This project has received funding from the European Research Council (ERC) under the European Union's Horizon 2020 research and innovation programme under grant agreement No. 714605.

Supplementary materials

Supplementary material associated with this article can be found, in the online version, at doi:10.1016/j.combustflame.2021.02.012.

References

[1] T. Lu, C.K. Law, Toward accommodating realistic fuel chemistry in large-scale computations, Prog. Energy Combust. Sci. 35 (2009) 192–215.
[2] PrIMe, http://primekinetics.org.
[3] ReSpecTh, http://respecth.chem.elte.hu/respecth/index.php.
[4] H.J. Curran, Developing detailed chemical kinetic mechanisms for fuel combustion, Proc. Combust. Inst. 37 (2019) 57–81.
[5] S.J. Klippenstein, From theoretical reaction dynamics to chemical modeling of combustion, Proc. Combust. Inst. 36 (2017) 77–111.
[6] T. Faravelli, F. Manenti, E. Ranzi, Mathematical Modelling of Gas-Phase Complex Reaction Systems: Pyrolysis and Combustion, Elsevier, 2019.
[7] N. Vandewiele, K. Van Geem, M.-F. Reyniers, G. Marin, Genesys: kinetic model construction using chemo-informatics, Chem. Eng. J. 207–208 (2012) 526–538.
[8] R. de Vijver, J. Zádor, KinBot: automated stationary point search on potential energy surfaces, Comput. Phys. Commun. 248 (2020) 106947.
[9] A. Rodríguez, R. Rodríguez-fernández, S.A. Vázquez, G.L. Barnes, J.J.P. Stewart, E. Martínez-núñez, tsscds2018 : a code for automated discovery of chemical reaction mechanisms and solving the kinetics, J. Comput. Chem. 39 (2018) 1922–1930.
[10] P.L. Bhoorasingh, B.L. Slakman, F.S. Khanshan, J.Y. Cain, R.H. West, Automated transition state theory calculations for high- throughput kinetics, J. Phys. Chem. 121 (2017) 6896–6904.
[11] M. Keçeli, S.N. Elliott, Y. Li, M.S. Johnson, C. Cavallotti, Y. Georgievskii, W.H. Green, M. Pelucchi, J.M. Wozniak, A.W. Jasper, S.J. Klippenstein, Automated computational thermochemistry for butane oxidation : a prelude to predictive automated combustion kinetics, Proc. Combust. Inst. 37 (2019) 363–371.
[12] M. Frenklach, Transforming data into knowledge—process Informatics for combustion chemistry, Proc. Combust. Inst. 31 (2007) 125–140.
[13] E. Ranzi, A. Frassoldati, R. Grana, A. Cuoci, T. Faravelli, A.P. Kelley, C.K. Law, Hierarchical and comparative kinetic modeling of laminar flame speeds of hydrocarbon and oxygenated fuels, Prog. Energy Combust. Sci. 38 (2012) 468–501.
[14] S.W. Benson, Thermochemical Kinetics. Methods for the Estimation of Thermochemical Data and Rate Parameters, John Wiley & Sons, Ltd, 1976.
[15] D.L. Baulch, M.J. Pilling, C.J. Cobos, R.A. Cox, P. Frank, G. Hayman, T. Just, J.A. Kerr, T. Murrells, J. Troe, R.W. Walker, J. Warnatz, Evaluated kinetic data for combustion modeling. Supplement II, J. Phys. Chem. Ref. Data 34 (2005) 757–1397.
[16] A.S. Tomlin, The role of sensitivity and uncertainty analysis in combustion modelling, Proc. Combust. Inst. 34 (2013) 159–176.
[17] C.K. Westbrook, F.L. Dryer, Chemical kinetics and modeling of combustion processes, Proc. Combust. Inst. 18 (1981) 749–767.
[18] S.J. Klippenstein, L.B. Harding, P. Glarborg, J.A. Miller, The role of NNH in NO formation and control, Combust. Flame 158 (2011) 774–789.
[19] C.F. Goldsmith, A.S. Tomlin, S.J. Klippenstein, Uncertainty propagation in the derivation of phenomenological rate coefficients from theory: a case study of n-propyl radical oxidation, Proc. Combust. Inst. 34 (2013) 177–185.
[20] A. Stagni, C. Cavallotti, S. Arunthanayothin, O. Herbinet, F. Battin-Leclerc, T. Faravelli, An experimental, theoretical and kinetic modeling study of the gas-phase oxidation of ammonia, R. Soc. Chem. 5 (2020) 696–711.
[21] M.P. Burke, C.F. Goldsmith, S.J. Klippenstein, O. Welz, H. Huang, I.O. Antonov, J.D. Savee, D.L. Osborn, J. Za, C.A. Taatjes, L. Sheps, Multiscale informatics for low-temperature propane oxidation: further complexities in studies of complex reactions, J. Phys. Chem. 119 (2015) 7095–7115.
[22] M.P. Burke, S.J. Klippenstein, L.B. Harding, A quantitative explanation for the apparent anomalous temperature dependence of $OH+HO_2=H_2O+O_2$ through multi-scale modeling, Proc. Combust. Inst. 34 (2013) 547–555.
[23] R.J. Shannon, A.S. Tomlin, S.H. Robertson, M.A. Blitz, M.J. Pilling, P.W. Seakins, Global uncertainty propagation and sensitivity analysis in the $CH_3OCH_2+O_2$ system: combining experiment and theory to constrain key rate coefficients in DME combustion, J. Phys. Chem. 119 (2015) 7430–7438.
[24] D.R. Glowacki, C.H. Liang, C. Morley, M.J. Pilling, S.H. Robertson, MESMER: an open-source master equation solver for multi-energy well reactions, J. Phys. Chem. A 116 (2012) 9545–9560.
[25] M. Frenklach, H. Wang, M.J. Rabinowitz, Optimization and analysis of large chemical kinetic mechanisms using the solution mapping method – combustion of methane, Prog. Energy Combust. Sci. 18 (1992) 47–73.
[26] M. Frenklach, H. Wang, M. Goldenberg, G.P. Smith, D.M. Golden, GRI-MECH: An an Optimized Detailed Chemical Reaction Mechanism for Methane Combustion, 1995 Topical report, September 1992-August 1995United States.
[27] M. Frenklach, A. Packard, P. Seiler, R. Feeley, Processing in developing predictive models of complex reaction systems, Int. J. Chem. Kinet. 36 (2003) 57–66.
[28] R. Feeley, P. Seiler, A. Packard, M. Frenklach, Consistency of a reaction dataset, J. Phys. Chem. 108 (2004) 9573–9583.
[29] T. Russi, A. Packard, R. Feeley, M. Frenklach, Sensitivity analysis of uncertainty in model prediction, J. Phys. Chem. 112 (2008) 2579–2588.
[30] T. Russi, A. Packard, M. Frenklach, Uncertainty quantification : making predictions of complex reaction systems reliable, Chem. Phys. Lett. 499 (2010) 1–8.
[31] X. You, T. Russi, A. Packard, M. Frenklach, Optimization of combustion kinetic models on a feasible set, Proc. Combust. Inst. 33 (2011) 509–516.
[32] M. Frenklach, A. Packard, G. Garcia-donato, R. Paulo, J. Sacks, Comparison of statistical and deterministic frameworks of uncertainty quantification, SIAM/ASA J. Uncertain. Quantif. 4 (2016) 875–901.
[33] N.A. Slavinskaya, M. Abbasi, J.H. Starcke, R. Whitside, A. Mirzayeva, U. Riedel, W. Li, J. Oreluk, A. Hegde, A. Packard, M. Frenklach, G. Gerasimov, O. Shatalov, Development of an uncertainty quantification predictive chemical reaction model for syngas combustion, Energy Fuels 31 (2017) 2274–2297.
[34] S. Iavarone, J. Oreluk, S.T. Smith, A. Hegde, W. Li, A. Packard, M. Frenklach, P.J. Smith, F. Contino, A. Parente, Application of bound-to-bound data collaboration approach for development and uncertainty quantification of a reduced char combustion model, Fuel 232 (2018) 769–779.
[35] L. Elliott, D.B. Ingham, A.G. Kyne, N.S. Mera, M. Pourkashanian, C.W. Wilson, Genetic algorithms for optimisation of chemical kinetics reaction mechanisms, Prog. Energy Combust. Sci. 30 (2004) 297–328.
[36] T. Turányi, T. Nagy, I.G. Zsély, M. Cserháti, T. Varga, B.T. Szabó, I. Sedyó, P.T. Kiss, A. Zempléni, H.J. Curran, Determination of rate parameters based on both direct and indirect measurements, Int. J. Chem. Kinet. 44 (2012) 284–302.
[37] T. Varga, T. Nagy, C. Olm, I.G. Zsély, R. Pálvölgyi, G.V. Valkó, M. Cserháti, H.J. Curran, T. Turányi, Optimization of a hydrogen combustion mechanism using both direct and indirect measurements, Proc. Combust. Inst. 35 (2015) 589–596.
[38] M. Kovács, M. Papp, I.G. Zsély, T. Turányi, Determination of rate parameters of key N/H/O elementary reactions based on H_2/O_2/NOx combustion experiments, Fuel 264 (2020) 116720.
[39] T. Varga, C. Olm, T. Nagy, I.G. Zsély, É. Valkó, R. Pálvölgyi, H.J. Curran, T. Turányi, Development of a joint hydrogen and syngas combustion mechanism based on an optimization approach, Int. J. Chem. Kinet. 48 (2016) 407–422.
[40] C. Olm, T. Varga, É. Valkó, H.J. Curran, T. Turányi, Uncertainty quantification of a newly optimized methanol and formaldehyde combustion mechanism, Combust. Flame. 186 (2017) 45–64.
[41] C. Olm, T. Varga, É. Valkó, S. Hartl, C. Hasse, T. Turányi, Development of an ethanol combustion mechanism based on a hierarchical optimization approach, Int. J. Chem. Kinet. 48 (2016) 423–441.
[42] H.N. Najm, B.J. Debusschere, Y.M. Marzouk, S. Widmer, Uncertainty quantification in chemical systems, Int. J. Numer. Method Eng. 80 (2009) 789–814.
[43] D.A. Sheen, H. Wang, The method of uncertainty quantification and minimization using polynomial chaos expansions, Combust. Flame 158 (2011) 2358–2374.
[44] H. Wang, D.A. Sheen, Combustion kinetic model uncertainty quantification, propagation and minimization, Prog. Energy Combust. Sci. 47 (2015) 1–31.
[45] L. Cai, H. Pitsch, Mechanism optimization based on reaction rate rules, Combust. Flame 161 (2014) 405–415.
[46] Reaction Design: San Diego, ANSYS Chemkin theory manual 17.0 (15151), (2015).
[47] A. Evans, V. Strezov, T.J. Evans, Assessment of utility energy storage options for increased renewable energy penetration, Renew. Sustain. Energy Rev. 16 (2012) 4141–4147.
[48] H. Kobayashi, A. Hayakawa, K.D.K.A. Somarathne, E.C. Okafor, Science and technology of ammonia combustion, Proc. Combust. Inst. 37 (2019) 109–133.
[49] L. Appels, J. Baeyens, J. Degrève, R. Dewil, Principles and potential of the anaerobic digestion of waste-activated sludge, Prog. Energy Combust. Sci. 34 (2008) 755–781.
[50] D.P.B.T.B. Strik, A.M. Domnanovich, P. Holubar, A pH-based control of ammonia in biogas during anaerobic digestion of artificial pig manure and maize silage, Process Biochem. 41 (2006) 1235–1238.
[51] C. Lhuillier, P. Brequigny, N. Lamoureux, F. Contino, C. Mounaïm-Rousselle, Experimental investigation on laminar burning velocities of ammonia/hydrogen/air mixtures at elevated temperatures, Fuel 263 (2020) 116653.
[52] A. Valera-Medina, R. Marsh, J. Runyon, D. Pugh, P. Beasley, T. Hughes, P. Bowen, Ammonia–methane combustion in tangential swirl burners for gas turbine power generation, Appl. Energy 185 (2017) 1362–1371.
[53] H. Kobayashi, A. Hayakawa, K.D.K.A. Somarathne, E.C. Okafor, Science and technology of ammonia combustion, Proc. Combust. Inst. (2018) 1–25.
[54] R. Li, A.A. Konnov, G. He, F. Qin, D. Zhang, Chemical mechanism development and reduction for combustion of $NH_3/H_2/CH_4$ mixtures, Fuel 257 (2019) 116059.

[55] O. Mathieu, E.L. Petersen, Experimental and modeling study on the high-temperature oxidation of Ammonia and related NOx chemistry, Combust. Flame 162 (2015) 554–570.
[56] K.P. Shrestha, L. Seidel, T. Zeuch, F. Mauss, Detailed kinetic mechanism for the oxidation of ammonia including the formation and reduction of nitrogen oxides, Energy Fuels 32 (2018) 10202–10217.
[57] P. Glarborg, J.A. Miller, B. Ruscic, S.J. Klippenstein, Modeling nitrogen chemistry in combustion, Prog. Energy Combust. Sci. 67 (2018) 31–68.
[58] T. Varga, C. Olm, T. Nagy, I.G. Zsély, É. Valkó, R. Pálvölgyi, H.J. Curran, T. Turányi, Development of a joint hydrogen and syngas combustion mechanism based on an optimization approach, Int. J. Chem. Kinet. 48 (2016) 407–422.
[59] Y. Tao, H. Wang, Joint probability distribution of Arrhenius parameters in reaction model optimization and uncertainty minimization, Proc. Combust. Inst. 37 (2019) 817–824.
[60] M.S. Bernardi, M. Pelucchi, A. Stagni, L.M. Sangalli, A. Cuoci, A. Frassoldati, P. Secchi, T. Faravelli, Curve matching, a generalized framework for models/experiments comparison: an application to n-heptane combustion kinetic mechanisms, Combust. Flame 168 (2016) 186–203.
[61] M. Pelucchi, A. Stagni, T. Faravelli, Chapter 15 – Addressing the complexity of combustion kinetics: data management and automatic model validation, in: T. Faravelli, F. Manenti, E.B.T.-C.A.C.E. Ranzi (Eds.), Math. Model. Gas-Phase Complex React. Syst. Pyrolysis Combust., Elsevier (2019), pp. 763–798.
[62] http://hdl.handle.net/2013/ULB-DIPOT:oai:dipot.ulb.ac.be:2013/307514.
[63] T. Turányi, T. Nagy, I.G. Zsély, M. Cserháti, T. Varga, B.T. Szabó, I. Sedyó, P.T. Kiss, A. Zempléni, H.J. Curran, Determination of rate parameters based on both direct and indirect measurements, Int. J. Chem. Kinet. 44 (2012) 284–302.
[64] M. Schwaab, J.C. Pinto, Optimum reference temperature for reparameterization of the Arrhenius equation . Part 1 : problems involving one kinetic constant, Chem. Eng. Sci. 62 (2007) 2750–2764.
[65] M. Schwaab, L.P. Lemos, J.C. Pinto, Optimum reference temperature for reparameterization of the Arrhenius equation . Part 2 : problems involving multiple reparameterizations, Chem. Eng. Sci. 63 (2008) 2895–2906.
[66] T. Nagy, T. Turányi, Uncertainty of Arrhenius parameters, Int. J. Chem. Kinet. 43 (2011) 359–378.
[67] T. Nagy, T. Turányi, Determination of the uncertainty domain of the Arrhenius parameters needed for the investigation of combustion kinetic models, Reliab. Eng. Syst. Saf. 107 (2012) 29–34.
[68] T. Nagy, É. Valkó, I. Sedyó, I.G. Zsély, M.J. Pilling, T. Turányi, Uncertainty of the rate parameters of several important elementary reactions of the H2 and syngas combustion systems, Combust. Flame 162 (2015) 2059–2076.
[69] M.B. Fürst, P. Sabia, M. Lubrano Lavadera, G. Aversano, M. De Joannon, A. Frassoldati, A. Parente, Optimization of chemical kinetics for methane and biomass pyrolysis products in MILD combustion, Energy Fuels 32 (2018) 10194–10201.
[70] J.S.U. Hjorth, Computer Intensive Statistical Methods: Validation Model Selection and Bootstrap, CRC Press, London, 1993.
[71] C. Olm, I.G. Zsély, T. Varga, H.J. Curran, T. Turányi, Comparison of the performance of several recent syngas combustion mechanisms, Combust. Flame 162 (2015) 1793–1812.
[72] B.M. Adams, W.J. TBohnhoff, K.R. Dalbey, J.P. Eddy, M.S. Eldred, D.M. Gay, K. Haskell, P.D. Hough, L.P. Swiler, DAKOTA, a Multilevel Parallel Object-Oriented Framework for Design Optimization, Parameter Estimation, Uncertainty Quantification, and Sensitivity Analysis: Version 5.0 User's Manual, Sandia National Laboratories, 2009 Tech. Rep. SAND2010-2183.
[73] A. Cuoci, A. Frassoldati, T. Faravelli, E. Ranzi, OpenSMOKE++: an object-oriented framework for the numerical modeling of reactive systems with detailed kinetic mechanisms, Comput. Phys. Commun. 192 (2015) 237–264.
[74] A. Cuoci, A. Frassoldati, T. Faravelli, E. Ranzi, Numerical modeling of laminar flames with detailed kinetics based on the operator-splitting method, Energy Fuels 27 (2013) 7730–7753.
[75] C.J. Cobos, H. Hippler, J. Troe, Experimental and numerical study, under LTC conditions, of ammonia ignition delay with and without hydrogen addition, J. Phys. Chem. 89 (1985) 342–349.
[76] J. Troe, Detailed modeling of the temperature and pressure dependence of the reaction H + O_2 (+M) → HO2 (+M), Proc. Combust. Inst. 28 (2000) 1463–1469.
[77] B. Shu, S.K. Vallabhuni, X. He, G. Issayev, K. Moshammer, A. Farooq, R.X. Fernandes, A shock tube and modeling study on the autoignition properties of ammonia at intermediate temperatures, Proc. Combust. Inst. 37 (2019) 205–211.
[78] X. He, B. Shu, D. Nascimento, K. Moshammer, M. Costa, R.X. Fernandes, Auto-ignition kinetics of ammonia and ammonia/hydrogen mixtures at intermediate temperatures and high pressures, Combust. Flame 206 (2019) 189–200.
[79] M. Pochet, V. Dias, B. Moreau, F. Foucher, H. Jeanmart, F. Contino, Experimental and numerical study, under LTC conditions, of ammonia ignition delay with and without hydrogen addition, Proc. Combust. Inst. (2018) 1–9.
[80] V.J. Wargadalam, G. Löffler, F. Winter, H. Hofbauer, Homogeneous formation of NO and N_2O from the oxidation of HCN and NH_3 at 600–1000°C, Combust. Flame 2180 (2000) 465–478.
[81] Y. Song, H. Hashemi, J.M. Christensen, C. Zou, P. Marshall, P. Glarborg, Ammonia oxidation at high pressure and intermediate temperatures, Fuel 181 (2016) 358–365.
[82] D.F. Davidson, K. Kohse-Höinghaus, A.Y. Chang, R.K. Hanson, A pyrolysis mechanism for ammonia, Int. J. Chem. Kinet. 22 (1990) 513–535.
[83] P.D. Ronney, Effect of chemistry and transport properties on near-limit flames at microgravity, Combust. Sci. Technol. 59 (1988) 123–141.
[84] R. Rota, D. Antos, E.F. Zanoelo, S. Carra, Experimental study and kinetic modelling of nitric oxide reduction with ammonia, Combust. Sci. Technol. 163 (2001) 25–47.
[85] P. Dagaut, Experimental and kinetic modeling study of the effect of SO_2 on the reduction of NO by ammonia, Proc. Combust. Inst. 30 (2005) 1211–1218.
[86] C. Lee, S. Vranckx, K.A. Heufer, S.V. Khomik, Y. Uygun, H. Olivier, R.X. Fernandes, On the chemical kinetics of ethanol oxidation: shock tube, rapid compression machine and detailed modeling study, Z. Phys. Chem. 226 (2012) 1–27.
[87] C.J. Sung, H.J. Curran, Using rapid compression machines for chemical kinetics studies, Prog. Energy Combust. Sci. 44 (2014) 1–18.
[88] J. Warnatz, Resolution of gas phase and surface combustion chemistry into elementary reactions, Symp. Combust. 24 (1992) 553–579.
[89] L. Zalotai, T. Be, Effect of the uncertainty of kinetic and thermodynamic data on methane flame simulation results, Phys. Chem. Chem. Phys. 4 (2002) 2568–2578.
[90] C. Cavallotti, M. Pelucchi, Y. Georgievskii, S.J. Klippenstein, EStokTP: electronic structure to temperature- and pressure-dependent rate constants-A code for automatically predicting the thermal kinetics of reactions, J. Chem. Theory Comput. 15 (2019) 1122–1145.
[91] A.M. Dean, J.W. Bozzelli, Gas-Phase Combustion Chemistry, W.C. Gardiner Jr. (Ed.), Springer, 2000.
[92] T.L. Nguyen, J.R. Barker, Sums and densities of fully coupled anharmonic vibrational states : a comparison of three practical methods, J. Phys. Chem. (2010) 3718–3730.
[93] J.V. Michael, J.W. Sutherland, R.B. Klemm, Rate constant for the reaction NH_3 over the temperature range, J. Phys. Chem. 90 (1986) 497–500.
[94] T. Ko, P. Marshall, A. Fontijn, Coefficients for the H+NH3 reaction over a wide temperature range, J. Phys. Chem. 94 (1990) 1401–1404.
[95] J. Li, H. Guo, A nine-dimensional global potential energy surface for NH4(X2A1) and kinetics studies on the $H+NH_3=H_2+NH_2$ reaction, Phys. Chem. Chem. Phys. 16 (2014) 6753–6763.
[96] J.R. Chen, H.Y. Tsai, J.H. Chien, H.J. Pan, Flow and flame visualization near the upper flammability limits of methane/air and propane/air mixtures at elevated pressures, J. Loss Prev. Process Ind. 24 (2011) 662–670.
[97] A. Bertolino, A. Stagni, A. Cuoci, T. Faravelli, A. Parente, A. Frassoldati, Prediction of flammable range for pure fuels and mixtures using detailed kinetics, Combust. Flame 207 (2019) 120–133.
[98] P. Glarborg, J.A. Miller, B. Ruscic, S.J. Klippenstein, Modeling nitrogen chemistry in combustion, Prog. Energy Combust. Sci. 67 (2018) 31–68.